Geochemistry of Iron–Calcium Hydroxophosphates in Pelagic Sediments: Origin and Compositional Evolution in the Course of Diagenesis

Article *in* Geochemistry International · June 2001

CITATIONS
15

READS
151

1 author:

Alexander V. Dubinin
P.P. Shirshov Institute of Oceanology
75 PUBLICATIONS **689** CITATIONS

SEE PROFILE

Geochemistry International, Vol. 39, No. 6, 2001, pp. 585–596. Translated from Geokhimiya, No. 6, 2001, pp. 645–657.

Geochemistry of Iron–Calcium Hydroxophosphates in Pelagic Sediments: Origin and Compositional Evolution in the Course of Diagenesis

A. V. Dubinin

Shirshov Institute of Oceanology, Russian Academy of Sciences, Nakhimovskii pr. 36, Moscow, 117851 Russia
e-mail: geochem@geo.sio.rssi.ru

Received August 9, 1999

Abstract— A phase consisting of iron, phosphorus, and calcium was found in pelagic sediments for the first time. This phase was referred to as iron–calcium hydroxophosphates. They were isolated from the >50 μm fraction of eupelagic clays sampled at Station 35, which was located in the South Pacific Depression. The iron–calcium hydroxophosphates are encountered both as clastics or nodules and as inclusions in phillipsites.

The bulk composition of the >50 μm phillipsite fraction from four eupelagic clay horizons (burial depths 37–40, 105–110, 165–175, and 189–190 cm) showed that the abundances of iron, calcium, and tervalent rare-earth elements (REE) correlate with phosphorus: they increase with increasing hydrothermal matter fraction in the sediment. Therefore, presumably, iron–calcium hydroxophosphates are hydrothermal in origin. Electron probe microanalysis showed a variable composition of iron–calcium hydroxophosphates from the upper two sampled horizons (burial depths 37–40 and 105–110 cm). The molar ratio P : Ca approximates 0.6, as in apatite, and iron becomes more abundant with decreasing in-grain calcium and phosphorus concentrations. X-ray powder diffraction showed that iron–calcium hydroxophosphates were fine, submicron intergrowths of apatite and goethite aggregates (at burial depths 105–110 cm) or of high-phosphorus goethite (at burial depths 37–40 cm). The absence of iron–calcium hydroxophosphates in the two ancient sediment horizons, in spite of a tight association between iron, calcium, and phosphorus and of their increasing abundances, suggests that iron–calcium hydroxophosphates are unstable during diagenesis and that they decompose to goethite and apatite. The analysis of structural alterations experienced by iron–calcium hydroxophosphates showed that they changed with time from globular through cellular to massive structures. The iron is lost, and variations in the in-grain calcium and phosphorus abundances are reduced during this process.

Based on secondary-ion mass spectrometry (SIMS) evidence from two iron–calcium hydroxophosphate particles, REE accumulation (up to 400 ppm La), and cerium deficit were discovered. This suggests that the hydroxophosphates are generated in deep and/or near-floor oceanic water, that is, in the localities of submarine hydrothermal vents.

Rare-earth elements (REE) in deep-water, pelagic sediments are closely associated with phosphorus [1, 2]. An exception is cerium, which is accumulated in authigenous oxohydroxide sediments (ferromanganese crusts, nodules, micronodules). Data from consecutive leaching of bottom sediments show that bulk phosphorus is 61 to 86% biogenous apatite (bony detritus), 3 to 12% phosphorus can be associated with the organic matter, and 7 to 17% phosphorus is associated with iron oxohydroxides [3]. Maximum REE abundances are found in the highest phosphorus fractions (10–38 and 38–100 μm) [1]. The inspection of the temporal variation of the cerium anomaly showed that negative cerium anomalies are associated with the enrichment of the sediments by bony detritus [1, 4].

In ferromanganese crusts, the phosphorus fraction associated with iron oxohydroxides amounts to 41–91% [5]. In a hydrogenous ferromanganese crust from the South Pacific Depression, 84% phosphorus is associated with 36% iron oxohydroxides [6]. The mechanism of REE(III) accumulation in ferromanganese crusts, nodules, and micronodules can be interpreted as REE sorption and cosedimentation on iron oxohydroxides [7]. The REE composition of hydrogenous iron–manganese oxohydroxides is characterized by a positive cerium anomaly, which arises from cerium oxidation in surface oceanic water [8, 9]. The value of the cerium anomaly expressed as $Ce\ an = 2Ce/Ce^{NASC}/(La/La^{NASC} + Nd/Nd^{NASC})$, where NASC is North-American shale composite [10], is a direct function of cerium accumulation, and it decreases with increasing lanthanide(III) abundance. Under pelagic settings, variations in the cerium anomaly in ferromanganese crusts, nodules, and micronodules can be associated with either cerium accumulation or traces of a substance with a negative cerium anomaly [11–13]. Variations in calcium accumulation are characteristic of ferromanganese entities sampled from various sites in the ocean and differing

from one another by the extent of pelagicity (meaning the amount of lithogenous particles relative to the hydrogenous matter, the extent of the differentiation of REE composition of the particles and of the REE dissolved in the oceanic water, and other parameters). The variability of REE composition in ferromanganese oxohydroxide entities within a deep-water zone with similar sedimentation settings can be affected by the REE composition of other mineral phases.

During the study of ferromanganese nodules and host sediments of the radiolarian zone of the Pacific [14], it was discovered that REE and cerium in host sediments are associated with phosphorus (a P phase), and that variations in REE composition in ferromanganese nodules can arise from mixing the composition of the hypothetical P phase from the sediments with the composition of iron oxohydroxides (an Fe-phase). The P phase, which is characterized by a negative cerium anomaly, is compositionally similar to bony detritus [15].

Later studies of the composition of ferromanganese nodules and host sediments along the sedimentary column within the near-equator radiolarian zone of the Pacific [16] showed that the sediments had a negative cerium anomaly, that the tervalent REE abundances correlated with the phosphorus abundance in the reactive fraction of the sediment (1 M $NH_2OH \cdot HCl$ + 25% CH_3COOH extracts), and that the phosphorus recovery was a function of iron recovery. The involvement of the phase bearing iron and phosphorus in the composition of ferromanganese nodules causes local variability in the REE composition of floor nodules. The reason behind the local variability of ferromanganese nodules is the varied ratio of hydrogenous iron oxohydroxides to the Fe–P phase, the latter being iron hydroxophosphate or the phosphate ion sorbed on iron oxohydroxides [16].

The behavior of REE was studied in ferromanganese micro- and macronodules and host sediments from the bioproductive zones of the Pacific (radiolarian belt; Guatemalan and Peruvian depressions). The REE composition systematically changes from the smallest micronodules through larger ones to macronodules and finally to the reactive portion of the host sediment [11, 12, 17]. In all of the cases studied, the cerium anomaly was reduced in the order from micronodules to macronodules and to sediments; the fraction of the diagenetic matter, which was represented by iron oxohydroxides bearing sorbate phosphorus (iron hydroxophosphates), in ferromanganese nodules increased in the same order.

Particles represented by iron and iron–calcium hydroxophosphates are known to occur in fluvial and lacustrine water [18, 19]. There was no direct evidence for the existence of iron–calcium hydroxophosphates in oceanic suspended particles or sediments. By circumstantial evidence, the phosphate ions sorbed on iron oxohydroxides, like bony detritus, can enhance the considerable accumulation of REE, inheriting the negative cerium anomaly from the dissolved REE of oceanic waters. Iron hydroxophosphates are involved in postsedimentational processes; their presence in ferromanganese nodules decreases the cerium anomaly in the REE composition (diagenetic nodules of the radiolarian zone and Peruvian and Guatemalan depressions) [11, 12, 17].

High positive REE anomalies were observed in eupelagic clays from Sta. 35 located in the South Pacific Depression [20]. Later investigations showed that the REE content of the eupelagic clays from Sta. 35 increased down the column, together with the iron, manganese, and phosphorus abundances [21, 22]. The down-column growth in the iron and manganese abundances results from the increasing hydrothermal supply. The use of 1 M $NH_2OH \cdot HCl$ + 25% CH_3COOH and 3.5 N H_2SO_4 extracts showed high-phosphorus iron oxohydroxides in the sediments [6, 22]. The REE of ferromanganese micronodules and buried ferromanganese macronodules correlate with the phosphorus [23]. Iron–calcium hydroxophosphates were isolated with the <50 μm fraction of the sediments and appeared as traces in the phillipsite fraction, where their composition was studied.

The purpose of this study was to gain insight into iron–calcium hydroxophosphates first found in pelagic oceanic sediments. The origin and evolution of iron–calcium hydroxophosphates during burial will be considered on the basis of their chemical composition.

MATERIALS AND METHODS

A sediment column 190 cm long from Sta. 35, which was located in the Sough Pacific Depression (lat. 29°36′ S, long. 149°58′ W, water depth 3880 m) was sampled in 1980 during the 26th cruise of the R/V *Akademik Korolev* and was supplied by I.I. Volkov. In their upper portion, the sediments are represented by coccolithophera–foraminifera oozes (burial depths 0–10 cm). At deeper horizons (burial depths 10–12 cm), ferromanganese crusts were discovered to overlay oxidized eupelagic clays (burial depths 12–190 cm) with traces of the biogenous carbonate matter in separate horizons. A >50 μm fraction, mostly consisting of phillipsites, was sampled from four sediment horizons (burial depths 37–40, 105–110, 165–175, 189–190 cm). The phillipsites are represented by intergrowths coated with red-brown iron oxohydroxides. The phillipsites were analyzed as sampled without any chemical purification. The quality of the samples was controlled with a binocular microscope [22]. Despite this control, the microscopic examination of sectioned phillipsite samples showed, in addition to iron oxohydroxides, biogenous bony detritus, partially zeolitized volcanoclastics, and iron–calcium hydroxophosphates. The latter occurred as inclusions in phillipsites, cemented phillipsite crystals, or occurred as separate chips and concretions around phillipsite intergrowths (Figs. 1a–1d).

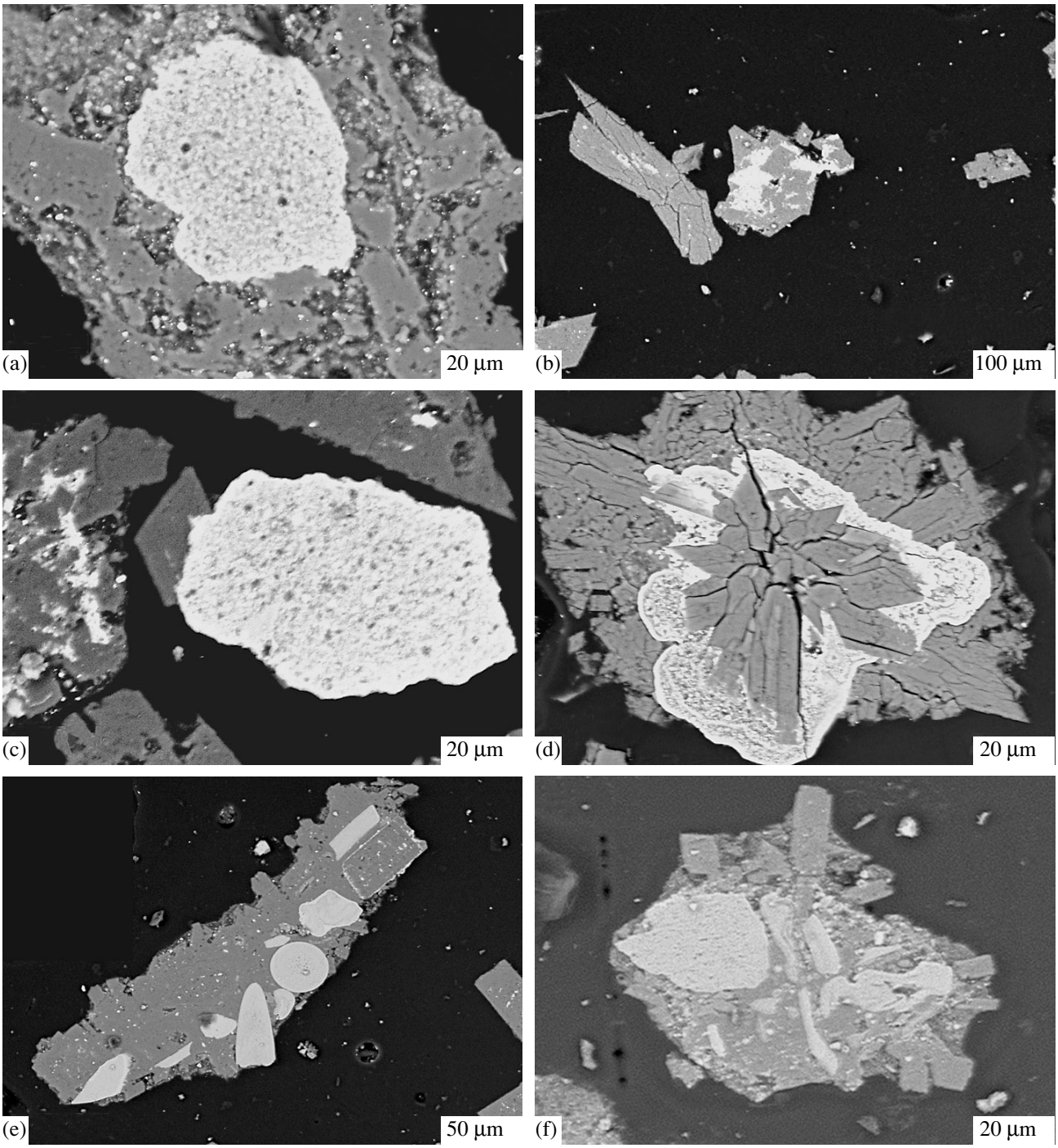

Fig. 1. Reflected-beam electron microphotographs of iron–calcium hydroxophosphates from eupelagic clays of the South Pacific Depression: (a) an iron–calcium hydroxophosphate inclusion in phillipsite (burial depths 37–40 cm); (b) cementation of phillipsite crystals by iron–calcium hydroxophosphates (light) (burial depths 105–110 cm); (c) an iron–calcium hydroxophosphate chip (light) surrounded by phillipsites, light spots in phillipsites are iron oxohydroxides (burial depths 105–110 cm); (d) concretion composed by iron–calcium hydroxophosphates around phillipsite intergrowths (burial depths 105–110 cm); (e) biogenous apatite (teeth) in a phillipsite grain (burial depths 165–175 cm); and (f) apatite chips (the large chip is suspected of being chemogenous in origin) in a phillipsite grain (burial depths 189–190 cm).

To analyze air-dry bulk phillipsite samples, samples of the >50 μm fraction 6–50 mg in size were treated by HF + $HClO_4$ in platinum bowls. The details of sample preparation are described elsewhere [23]. The REE, Th, W, Mo, Zr, and Hf were determined by inductively coupled plasma mass spectrometry [24, 25]. Fe, Mn, Co, Ni, Cu, Ca, Ti, and Al in the same samples were analyzed by flame atomic absorption. The precision of

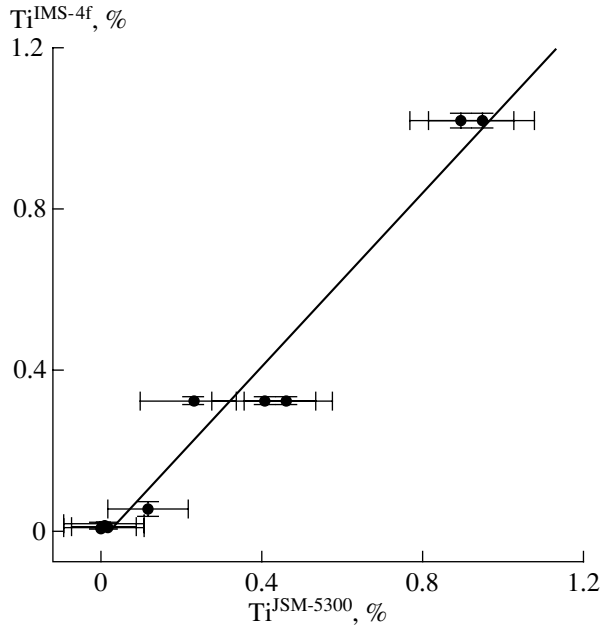

Fig. 2. Titanium percentage contents determined by SIMS (Ti^{IMS-4f}) versus titanium abundances derived by electron microprobe ($Ti^{JSM-5300}$) in iron–calcium hydroxophosphate (high-titanium) and phillipsite (low-titanium) samples. Regression equations: $y = 1.08x - 0.03$, $n = 9$, $r = 0.981$.

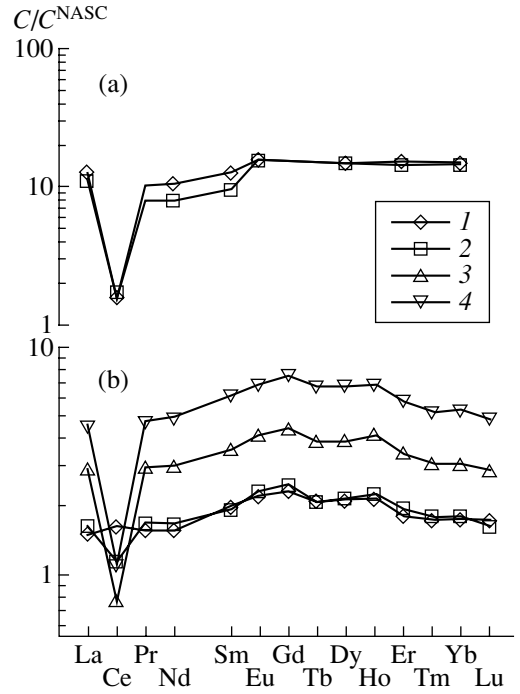

Fig. 3. REE compositions normalized to shale (NASC) [10] in (a) separate iron–calcium hydroxophosphate grains and (b) the >50 μm phillipsite fraction. Burial depths: (*1*) 37–40, (*2*) 105–110, (*3*) 165–175, and (*4*) 189–190 cm.

determinations ranged within 3–5 rel. %. Phosphorus was quantified by spectrophotometry. The analysis precision was 3 rel. %.

The chemical composition of iron–calcium hydroxophosphates was studied by means of a JSM-5300 electron microscope equipped with a Link ISIS attachment (IGEM Ross. Akad. Nauk). Test samples were graphitized sections. The detection limit for most elements was 0.08–0.10 wt %. The analysis precision (relative standard deviation) for Al, Si, and O was less than 3 rel. %; for K and Na, less than 8 rel. %; and for the other elements, it was within 20 rel. %.

The concentrations of eight REE (La, Ce, Nd, Sm, Eu, Dy, Er, Yb) and of Ba and Ti in two iron–calcium hydroxophosphate samples was measured by secondary-ion mass spectrometry (SIMS) on an IMS-4f ion-probe microanalyzer at the Institute of Microelectronics, Yaroslavl. Specimens prepared for electron-probe microanalysis were used. The abundance of an element was derived from the ratio of the appropriate isotope of the element to ^{30}Si. Experimental details are described elsewhere [26]. Because the secondary-ion mass spectrometry method of REE determination was originally designed for silicates, and because analytic specimens mainly consisted of the oxohydroxide–phosphate matrix, the analyses were verified by the titanium abundances measured by an electron probe and secondary ion mass spectrometry (Fig. 2). Despite the inhomogeneity of the hydroxophosphates, Fig. 2 makes it clear that the two methods give similar titanium abundances. The precision (relative standard deviation) of SIMS determination based on five replicate measurements at one site was better than 11–17 rel. % for REE(III) from burial depths 37–40 cm and better than 7 rel. % for Ce, Ti, and Ba. For a specimen from burial depths 105–110 cm, the analysis precision was better than 9 rel. % for all elements.

RESULTS OF THE ANALYSIS

The results of the analyses of bulk phillipsite samples of the >50 μm fraction are compiled in Table 1. The iron, phosphorus, calcium, and lanthanide(III) abundances increase down the sedimentary column, with practically invariable abundances of aluminum (7.71–8.73%) and titanium (0.16–0.19%; at burial depths of 189–190 cm, we were unable to determine titanium because of the small sample size. The cerium anomaly in the REE decreases down the column (Table 1, Fig. 3). The change in negative cerium anomaly down the column coincides with the variation in the cerium anomaly in the bulk sediment samples; this is related to the increasing hydrogenous fraction of the sediments [22].

Figure 4 shows iron, calcium, and REE(III) abundances plotted against phosphorus abundance in >50 μm bulk phillipsite samples. The variations in the abundances of these elements are not related to a change in phillipsite composition with the burial depth. Phillipsites do not change their composition with the burial depth as evi-

denced by an JSM-5300 electron microprobe with a Link ISIS attachment. Their composition can be expressed as $Na_{1.4–2.1}K_{1.6–1.9}Ca_{0.1–0.3}[Al_{4.1–4.3}Si_{10.5–11.2}O_{32}] \cdot 6H_2O$ [22]. Secondary-ion mass spectrometry showed that the tervalent REE abundance in phillipsite intergrowths varied from 0.1 to 18.1 ppm. These variations cannot interpret the observed trends in REE abundances and REE spectra in bulk phillipsite samples [27]. Therefore, the variations in the REE spectra and REE abundances arise from a trace mineral phase that contains calcium, phosphorus, and iron. A value approximating 3 : 2 : 1 was calculated for the molar ratio Ca : Fe : P in this phase. The Ca–P linear plot practically passes through the origin, indicating that almost all calcium is associated with phosphorus. Because the phosphorus does not enter phillipsites, a considerable fraction of the calcium is not likely associated with phillipsites. Evidence for this is the composition of the phillipsites, in which potassium and sodium are the major cations. A significant part of the iron is not associated with phosphorus and is likely iron oxohydroxide. Thus, the suggested chemical formula of iron–calcium hydroxophosphates can approximate $Ca_3Fe_2PO_4(OH)_9$ (Fig. 4).

A mineral phase with a similar composition was found in sectioned specimens of the >50 μm phillipsite fraction from burial depths 37–40 and 105–110 cm when they were examined with the JSM-5300 electron microscope equipped with the Link ISIS attachment (Fig. 1). The average compositions and the minimum and maximum abundances of the elements in iron–calcium hydroxophosphates in Table 2 are expressed in weight percentage. Because the total ranged from 72 to 100% as a function of the water content, for the ease of comparison we expressed all quantities in the text and figures in atomic percent.

Figure 5 depicts microphotographs of the iron–calcium hydroxophosphate specimen (Fig. 1c) in the Ca, Si, Fe, and P characteristic radiation. At the first glance, iron, phosphorus, and calcium are distributed uniformly over the hydroxophosphate chip. Actually, this is far from being true. A mosaic structure observed at small magnification (Fig. 1a) transforms to a globular one at high magnifications (Fig. 6a). Measuring the composition of globules at 12 points showed variations in the phosphorus abundance from 1.46 to 8.30 at. %. Together with the increasing phosphorus abundances, the calcium abundances increased and the iron abundances decreased.

Iron–calcium hydroxophosphate particles were discovered only at burial depths of 37–40 and 105–110 cm. The particles observed at burial depths of 37–40 cm had a globular or cellular structure (Fig. 6), while a cellular or massive structure was more frequent in the particles from burial depths of 105–110 cm (Fig. 7). A P–Fe–Ca ternary diagram distinctly shows that the particles encountered at burial depths of 105–110 cm are dominated by iron–calcium hydroxophosphates that are richer in phosphorus and calcium and poorer in iron.

Table 1. Abundances of elements in >50 μm phillipsite bulk samples in the sediments collected at Sta. 35

Element	Burial depth, cm			
	37–40	105–110	165–175	189–190
La	47.7	52.2	93.2	143
Ce	118	83.9	57.1	79.6
Pr	12.2	13.2	23.6	37.2
Nd	51.3	54.8	99.4	162
Sm	11.2	11.0	20.3	35.1
Eu	2.72	2.85	5.15	8.40
Gd	12.1	12.8	22.9	38.9
Tb	1.78	1.78	3.29	5.68
Dy	10.9	11.2	20.3	34.9
Ho	2.21	2.33	4.27	7.10
Er	6.14	6.58	11.8	19.7
Tm	0.86	0.89	1.54	2.60
Yb	5.39	5.53	9.53	16.4
Lu	0.82	0.78	1.39	2.31
Zr	90	40	26	75
Hf	2.7	0.8	0.6	1.7
Th	2.81	2.37	2.16	3.08
Mo	6.6	10	9	8.7
W	1.5	1.5	0.5	1.2
Fe	3.50	4.33	4.88	6.16
Mn	0.32	0.26	0.32	0.21
Al	8.59	8.73	8.63	7.71
Ti	0.19	0.17	0.16	<0.07
Co	0.009	0.003	<0.001	0.011
Ni	0.014	0.011	0.022	0.037
Cu	0.025	0.025	0.030	0.037
P	0.253	0.352	0.572	0.939
Ca	1.29	1.41	2.13	3.92
Mn/Fe	0.090	0.060	0.066	0.035
Ce an	1.07	0.70	0.26	0.23

Note: Abundances for REE, Th, Zr, Hf, Mo, and W are given in ppm; for the other elements, in percent.

The iron abundance of hydroxophosphate particles decreases in the following series of particle structures: globular ⇒ cellular ⇒ massive.

Based on Fig. 4, the trace mineral phase contained in phillipsites and consisting of phosphorus, iron, and calcium should almost entirely control the spectrum and abundance of REE in phillipsites. The rare-earth elements were measured by SIMS in two grains of iron–calcium hydroxophosphates from different burial depths. The results of the measurements are presented in Table 3, and the shale-normalized REE compositions are shown in Fig. 3. Figure 3 makes it clear that the

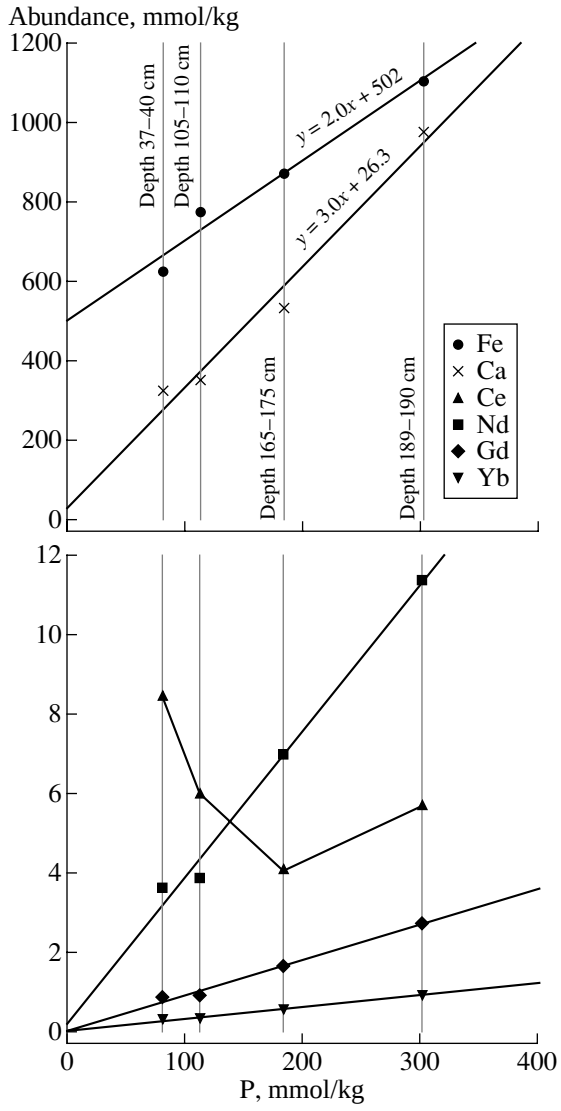

Fig. 4. Iron, calcium, and REE abundances versus phosphorus abundance as analyzed in the >50 μm phillipsite fraction.

REE spectra of the hydroxophosphates have a significant negative cerium anomaly, and that the REE abundances surpass those in both the phillipsite fraction and the bulk sediment samples [22]. This means that the phillipsite material and the sedimentary material are diluents for the REE of the hydroxophosphates.

RESULTS AND DISCUSSION

Origin of iron–calcium hydroxophosphates. A significant negative cesium anomaly in the REE composition of the hydroxophosphates, close in value to that observed in deep oceanic waters [28], may be evidence for the production of iron–calcium hydroxophosphates in near-bottom or deep oceanic waters. Downcolumn increases in iron, calcium, and phosphorus abundances in the >50 μm phillipsite fraction (Fig. 4) correlate with the iron and manganese contents increasing in the same direction and with the decreasing aluminum and silicon abundances in the bulk composition of the sediments [21, 22]. The criterion of the hydrothermal contribution to sediments, the Al : (Al + Fe + Mn) < 0.4 [29], changes systematically from 0.43 at burial depths of 20–25 cm to 0.20 at burial depths of 189–190 cm. Concurrent variations in the iron abundances in the phillipsite fraction and in the host sediment enabled us to suggest that the iron was entrained by the phillipsite fraction during sedimentation. Thus, a hydrogenous substance may be responsible for the regularities observed in the variation of iron abundances and in the associated variations in the phosphorus, calcium, and REE(III) abundances (Fig. 4).

Compositional variations of the hydrothermal suspended particles collected 19° S of the East Pacific Rise are shown in Fig. 7 as a ternary diagram in the P–Fe–Ca space. Data were taken from [30]. The composition of the particles follows a line that corresponds to the molar ratio P : Fe = 0.25. This (the highest possible) P : Fe value was derived from experiments on phosphorus accumulation during codeposition on iron hydroxide in seawater [31]. Figure 7 also shows the compositions of iron–calcium hydroxophosphates found at burial depths of 37–40 and 105–110 cm in sediments sampled at Sta. 35, which was located in the region of the South Pacific Depression. The hydroxophosphates show P : Ca of about 0.6. This phosphorus-to-calcium ratio correlates with the molar (atomic) ratio of these elements in apatite $Ca_{10}(PO_4)_6(OH)_2$. Particles with the highest hydrothermal contribution contain the maximum amount of iron. The field of the hydrothermal particle matter falls on the P : Ca = 0.6 line. This implies that, regarding the abundance ratio of P, Fe, and Ca, the hydrothermal particles may be the source of hydroxophosphates in the sediments in question.

The composition of iron–calcium hydroxophosphates is shown in Fig. 8 as compared to the average composition of the hydrothermal particulate matter (samples collected along the axis of the East Pacific Rise and at some distance from it), normalized to the background composition of the particles [30]. Evidently, apart from elevated aluminum and titanium abundances in iron–calcium hydroxophosphates, the abundances of other elements and abundance ratios are close to the hydrothermal particles sampled from the East Pacific Rise.

In addition to iron–calcium hydroxophosphates, iron oxohydroxides are abundant in the specimens studied. They are encountered in tight association with weathered volcanoclastics, along cleavage cracks, and between phillipsite intergrowths. Often, iron oxohydroxides decorate the boundaries of weathered volcanoclastic grains or form aureoles around zeolitization centers in volcanoclastics, being a product of its submarine destruction, like phillipsites (Fig. 1). Boundaries between iron oxohydroxides and iron–calcium hydrox-

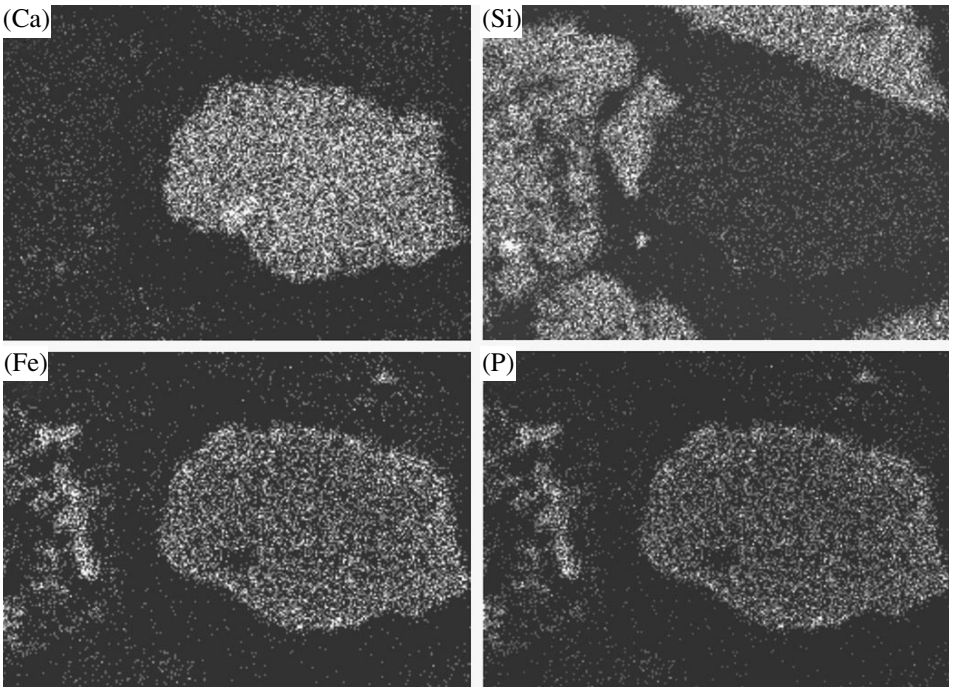

Fig. 5. Microphotographs of the iron–calcium hydroxophosphate chip from Fig. 1c in the Ca, Si, Fe, and P characteristic radiation.

ophosphates are quite conventional. The minimum phosphorus abundance found in iron–calcium hydroxophosphates is 1.51 wt %, and the maximum phosphorus abundance in iron oxohydroxides is 1.81 wt %. However, the fundamental distinction between iron oxohydroxides and iron–calcium hydroxophosphates is the existence of a significant direct correlation between phosphorus and iron in iron oxohydroxides and the existence of an inverse correlation in iron–calcium hydroxophosphates (Fig. 9). The reason behind the direct iron-to-phosphorus correlation in iron oxohydroxides is the sorption of phosphate ions from oceanic

Table 2. Average compositions and the minimal and maximal abundances of chemical elements in iron–calcium hydroxophosphates as found from 35 measurements. The compositions of biogenous (burial depths of 165–175 cm) and presumably chemogenous apatite (burial depths of 189–190 cm) are also presented

Component	Iron– calcium hydroxophosphate			Chemogenous apatite	Biogenous apatite
	average	minimum	maximum		
F	0.75	<0.10	1.99	2.20	2.81
Na_2O	0.61	<0.13	1.37	<0.10	0.77
MgO	2.33	0.33	4.03	<0.10	0.30
Al_2O_3	5.82	0.05	13.3	<0.10	0.10
SiO_2	7.01	0.10	32.0	<0.10	<0.17
P_2O_5	14.3	3.46	39.0	31.8	38.0
Cl	0.12	0.07	0.22	0.10	0.07
K_2O	0.43	<0.14	2.55	<0.10	<0.10
CaO	20.5	2.88	63.1	45.5	50.6
TiO_2	1.28	<0.12	2.69	<0.10	<0.18
MnO_2	0.83	<0.13	2.62	<0.10	0.03
Fe_2O_3	42.0	0.90	73.1	0.35	0.23
SrO	0.26	<0.07	1.08	<0.10	0.40

Note: Weight percentage abundances are presented.

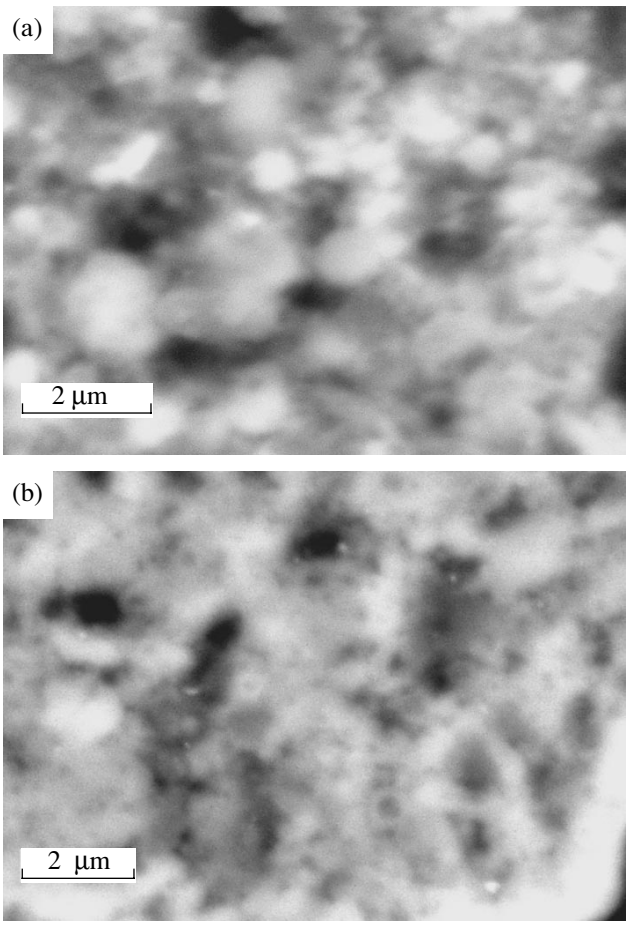

Fig. 6. Reflected-beam electron microphotographs of iron–calcium hydroxophosphates: (a) a globular structure of the sample imaged in Fig. 1a and (b) a cellular structure of a sample from burial depths 37–40 cm.

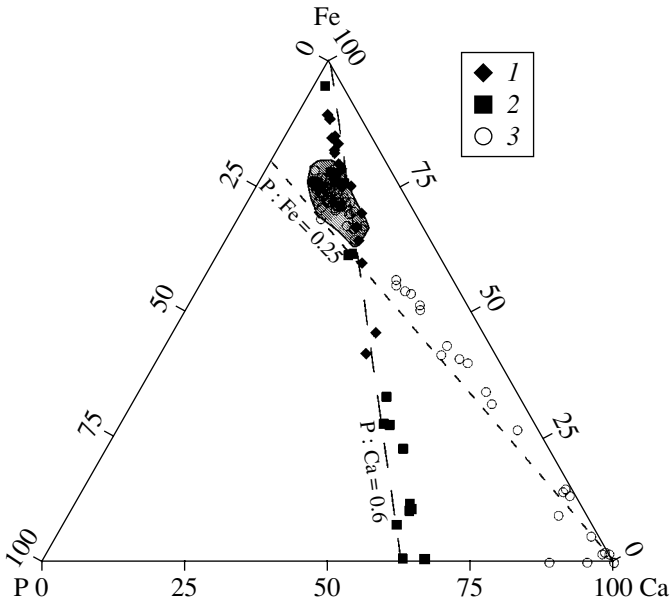

Fig. 7. Compositions of (*1*, *2*) iron–calcium hydroxophosphates from burial depths of (*1*) 37–40 cm and (*2*) 105–110 cm and (*3*) hydrogenous particles sampled in the region of 19° S at the East Pacific Rise [30] on the P–Ca–Fe ternary diagram. Lines show molar ratios P : Ca = 0.6 (apatite) and P : Fe = 0.25 (the highest ratio in experiments on the codeposition of phosphate ions from seawater by iron oxohydroxide [31]). The shaded field shows the highest iron content in the suspended particles.

water. As volcanoclastics weathering is enhanced, the accumulating oxohydroxide ions sorb phosphorus. The inverse iron-to-phosphorus correlation in iron–calcium hydroxophosphates is a result of the decomposition of iron–calcium hydroxophosphates to apatite and iron oxohydroxides (goethite).

Table 3. Abundances of REE, barium, and titanium in iron–calcium hydroxophosphates derived from SIMS

Element	Burial depth, cm	
	37–40	105–110
Ti	1.02	0.32
Ba	179	50
La	400	348
Ce	117	123
Nd	344	262
Sm	72	54
Eu	19	19
Dy	77	78
Er	51	49
Yb	45	44
Ce an	0.14	0.18

Note: For titanium, abundances are given in percent; for the other elements, abundances are given in ppm.

The behavior of aluminum and silicon relative to iron in samples of iron–calcium hydroxophosphates and iron oxohydroxides is demonstrated by Fig. 10. Iron in the oxohydroxides is in a negative correlation with silicon. This is a result of the higher mobility of silicon relative to iron during volcanoclastic weathering. The composition of iron oxohydroxide during weathering tends to reach FeOOH (goethite? 33 at. % Fe). Only one case is known where iron oxohydroxide was close in composition to hematite (burial depths of 189–190 cm, 40 at. % Fe).

Aluminum is less mobile than silicon in relation to the exportation of chemical elements during volcanoclastic weathering. Aluminum abundances in iron oxohydroxides decrease less significantly than silicon abundances (Fig. 10). If we assume that the degree of weathering of volcanic glass is controlled by the iron content in the form of oxohydroxide, the Si : Al ratio rapidly decreases with the progress of halmyrolysis. Although aluminum is a low-mobility element during sediment diagenesis, it is still more mobile than iron during volcanoclastic weathering. This is related to the fact that aluminum is employed as a precursor for phillipsite growth.

The Si : Al ratio in hydroxophosphates is practically invariable and is close to unity. With increasing iron

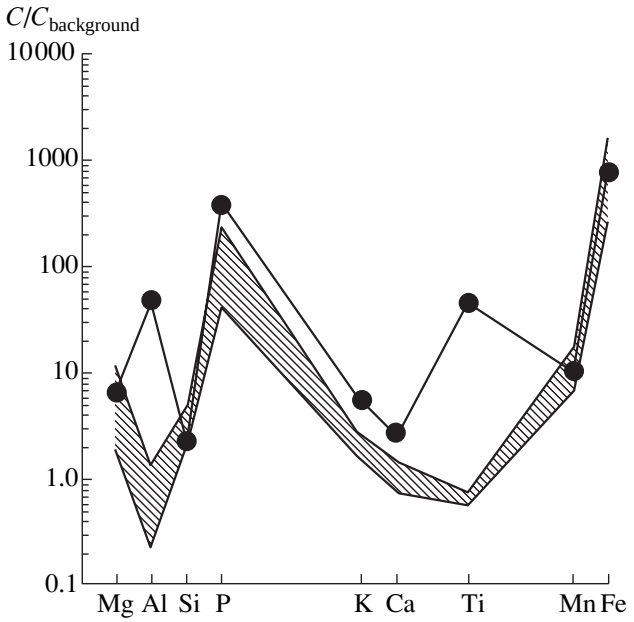

Fig. 8. Average composition of iron–calcium hydroxophosphates normalized to the composition of the reference particles collected from water depths 1000–2000 m [30]. The shaded field is confined to the compositions of the particles sampled on the axis of the East Pacific Rise (water depth 2300–2600 m) and at some distance from it (water depths 2350–2550 m).

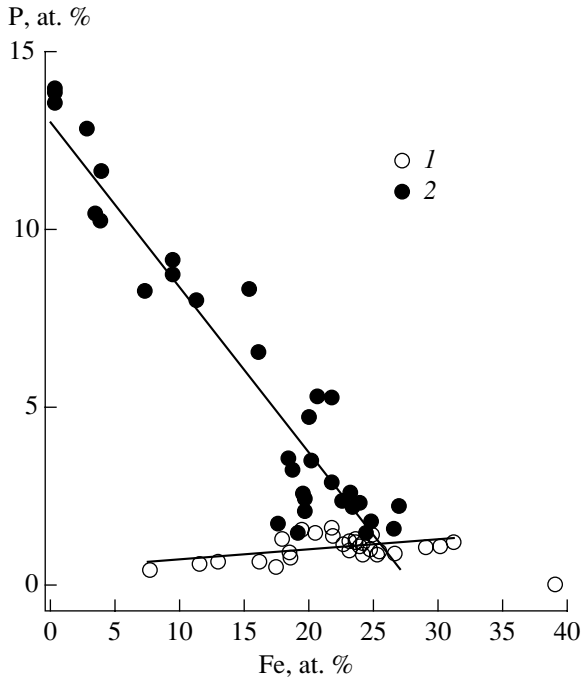

Fig. 9. Phosphorus abundance versus iron abundance in (*1*) iron oxohydroxides and (*2*) iron–calcium hydroxophosphates.

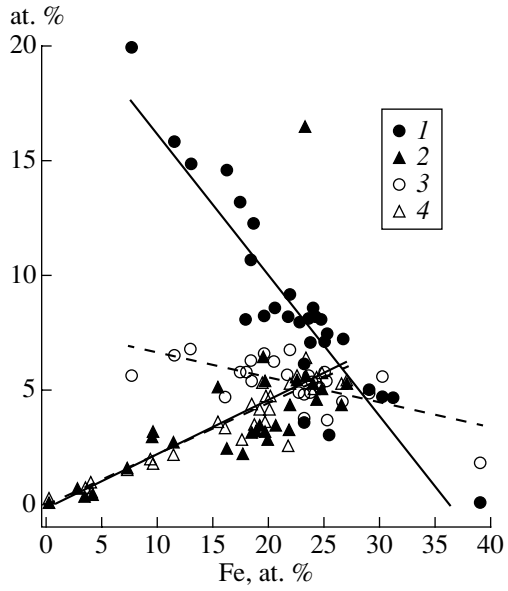

Fig. 10. (*1, 2*) Silicon abundance versus iron abundance in (*1*) iron oxohydroxides and (*2*) iron–calcium hydroxophosphates. (*3, 4*) Aluminum abundance versus iron abundance in (*3*) iron oxohydroxides and (*4*) iron–calcium hydroxophosphates.

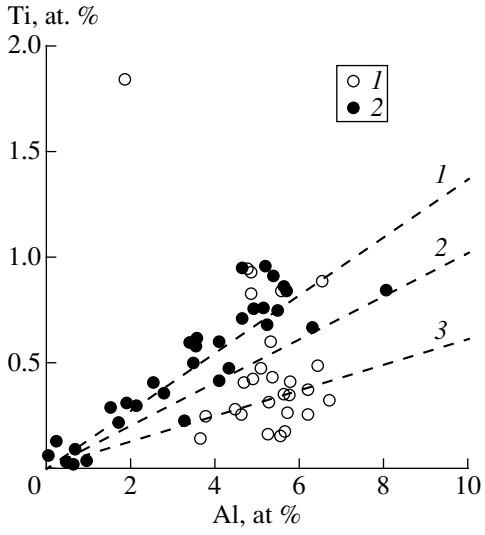

Fig. 11. Titanium abundance versus aluminum abundance in (*1*) iron oxohydroxides and (*2*) iron–calcium hydroxophosphates. Dashed lines show an atomic ratio Ti : Al equal to (*1*) 0.136 in reference particulate samples [30], (*2*) 0.101 in tholeiitic basalts from oceanic isles, and (*3*) 0.061 in tholeiitic basalts from oceanic ridges [33].

abundance, the aluminum and silicon abundances increase (Fig. 10). The simultaneous growth in the silicon and iron abundances occurs in hydrothermal particles. Aluminum accumulation in the particles was observed only in the highest iron specimens [30].

Titanium is among the least mobile elements during the halmyrolysis of basaltic glass [32]. The titanium abundance is plotted versus aluminum abundance in iron oxohydroxides and hydroxophosphates in Fig. 11. Clearly, the Ti : Al ratio in iron oxohydroxides is close

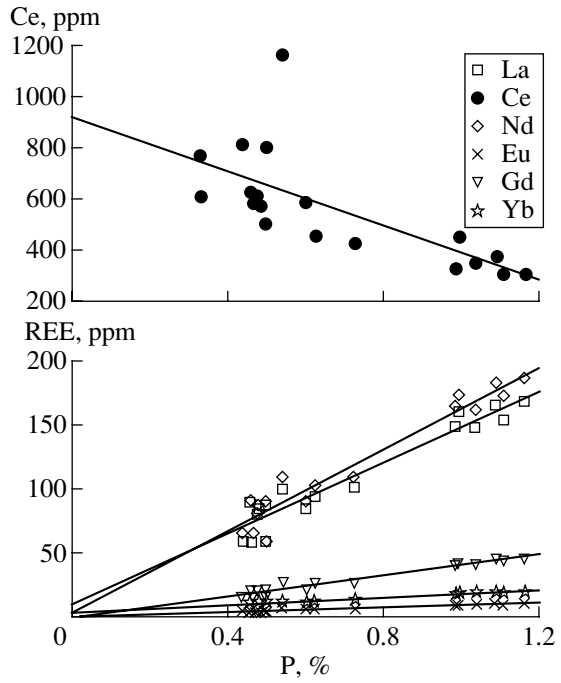

Fig. 12. REE abundance versus phosphorus abundance in ferromanganese micronodules and buried nodules from eupelagic clays sampled at Sta. 35.

to this ratio in tholeiitic basalts of midoceanic ridges and lower than in tholeiitic basalts from oceanic islands [33]. The Ti : Al ratio in the hydroxophosphates, equal to 0.133, is very similar to the value of 0.136 observed in reference particle specimens (water depths 1000–2000 m) from the East Pacific Rise [30]. A direct correlation of aluminum and titanium with iron and an inverse correlation of iron with phosphorus and calcium (Figs. 7, 9–11) are evidence that calcium phosphate acts as a type of diluent for iron oxohydroxide, because apatite does not accumulate these elements (Table 2).

Compositional evolution of iron–calcium hydroxophosphates during diagenesis. Figure 7 makes it clear that iron–calcium hydroxophosphates from the two burial depths differ in composition from each other. Hydroxophosphates from burial depths 37–40 cm are richer in iron and poorer in phosphorus and calcium. A similar phase from burial depths 105–110 cm shows wider compositional variations. Note that these variations can be observed in one iron–calcium hydroxophosphate grain. We regard this observation as an indication that the hydroxophosphates decompose with time to produce iron oxohydroxide and chemogenous apatite. As a result of this instability of iron–calcium hydroxophosphates, we have not found them in more ancient sedimentary horizons (burial depths 165–175 and 189–190 cm), in spite of bulk analysis data for the >50 μm phillipsite fraction (Table 1, Fig. 4). We met apatite as inclusions in phillipsites at these burial depths, which differed from biogenous apatites by the absence of characteristic toothlike forms (Figs. 1e, 1f). The composition of such apatite found in Table 2 shows that chemogenous apatite is indistinguishable from the biogenous one.

High magnifications make it clear that iron–calcium hydroxophosphates can have a globular, cellular (Fig. 6), or massive texture. The first two structure types are characteristic of hydroxophosphates from burial depths of 37–40 cm; the last two, from burial depths of 105–110 cm. If wide between-globule phosphorus variations (1.46–8.30 at. %) are associated with globular structures, the other two structures show reduced variation ranges together with an elevated lower bound of the phosphorus abundance (3.56–6.53 and 10.2–13.8 at. %, respectively). The iron abundance systematically decreases at the same time (15.5–27.0 $\Rightarrow$ 16.1–20.1 $\Rightarrow$ 0.3–4.1). In other terms, iron–calcium hydroxophosphates decompose with time to separate iron oxohydroxides.

These observations are supported by the thermodynamic calculations of the stability of iron phosphate $FePO_4$ and solid solutions of iron phosphates in iron hydroxide [18]. In the environment of deep-water or near-bottom oceanic waters and of pore solutions, iron hydroxides will be a stable phase at pH 7.5–8 and phosphate concentration averaging 3 μmol/l. Consequently, the metastable iron–calcium hydroxophosphates produced in deep oceanic water through phosphate sorption–cosedimentation by hydrothermal iron oxohydroxide will finally decompose to iron oxohydroxide and calcium phosphate. T.Yu. Uspenskaya reported that X-ray phase analysis showed iron–calcium hydroxophosphate from burial depths of 105–110 cm (Fig. 1c) to consist of fine, submicron aggregates of apatite and goethite. However, only goethite was identified in a hydroxophosphate specimen from burial depths of 37–40 cm (Fig. 1a).

The molar ratio Fe : Ca : P in the hydrothermal particles is 5.8 : 0.7 : 1; in the sediments this ratio averages 2.7 : 1.7 : 1 (Table 2). Finally, the decomposition of iron–calcium hydroxophosphates results in goethite and apatite by the reactions

$$\underset{\text{suspension}}{Fe_{5.8}Ca_{0.7}PO_4(OH)_{15.9}} + Ca^{2+}_{sol} + 1.9(OH)^-$$

$$\Rightarrow \underset{\text{sediment}}{Fe_{2.7}Ca_{1.7}PO_4(OH)_{8.5}} + 3.1Fe(OH)_3,$$

$$\underset{\text{sediment}}{6Fe_{2.7}Ca_{1.7}PO_4(OH)_{8.5}}$$

$$\Rightarrow 16.2Fe(OH)_3 + \underset{\text{sediment}}{Ca_{10}(PO_4)_6(OH)_2}.$$

The particles are clearly depleted in calcium relative to sedimentary iron–calcium hydroxophosphates; the calcium-to-phosphorus ratio in the sedimentary

hydroxophosphates is practically equal to that in apatite.

Likely, the iron oxohydroxide released upon hydroxophosphate decomposition, being involved in ferromanganese nodule and micronodule generation, involves hydroxophosphates in them. A concretion centered by a phillipsite intergrowth is discovered at burial depths of 105–110 cm (Fig. 1d). Almost pure (the lightest) goethite with 0.75 wt % P and 0.45 wt % Mn was found between grains. The outer layer is iron oxohydroxide with up to 1.8 wt % Mn and up to 1 wt % P. The inner portion of the concretion approaches iron–calcium hydroxophosphates (mosaic structures) with 2.1–3 wt % P.

Hydroxophosphates are involved in ferromanganese micro- and macronodules. High REE(III) abundances in hydroxophosphates result in correlation relations between REE(III) and phosphorus in ferromanganese oxohydroxide entities of sediments from Sta. 35 (Fig. 12). The iron and phosphorus abundances in the bulk composition of sediments rise down the eupelagic clay column. The higher the hydroxophosphate content of the sediment is, the higher this content of ferromanganese nodules and micronodules. Phase analysis shows that the iron–calcium hydroxophosphate abundance in sediments increases down the column, together with the iron and phosphorus abundances in buried ferromanganese nodules and micronodules [22, 23].

CONCLUSION

Iron–calcium hydroxophosphates have been found for the first time in pelagic oceanic sediments. They have been shown to originate during the sorption and cosedimentation of phosphate ions from oceanic waters on iron oxohydroxides. Iron–calcium hydroxophosphates accumulate significant amounts of tervalent REE. They have a negative cerium anomaly in the REE composition, which is characteristic of deep oceanic waters.

During diagenetic reactions in sediments, iron–calcium hydroxophosphates can transfer to ferromanganese oxohydroxide entities (nodules, micronodules). As a result, a correlation arises between the sedimentation of phosphorus and tervalent REE, and the cerium anomaly has its value changed.

Iron–calcium hydroxophosphates are present in oceanic sediments as a metastable phase. With time, they decompose to apatite and iron oxohydroxides in the course of diagenetic transformations.

ACKNOWLEDGMENTS

The help of V.N. Sval'nov and T.Yu. Uspenskaya is appreciated.

This study was supported by the Russian Foundation for Basic Research, project no. 97-05-64346, and that of Leading Scientific Schools, project no. 96-15-98440.

REFERENCES

1. Toyoda, K., Nakamura, Y., and Masuda, A., Rare Earth Elements of Pacific Pelagic Sediments, *Geochim. Cosmochim. Acta*, 1990, vol. 54, no. 4, pp. 1093–1103.
2. Strekopytov, S.V., Dubinin, A.V., and Volkov, I.I., General Regularities in the Behavior of Rare Earth Elements in Pacific Pelagic Sediments, *Litol. Polezn. Iskop.*, 1999, no. 2, pp. 133–145.
3. Filippelli, G.M. and Delaney, M.L., Phosphorus Geochemistry of Equatorial Pacific Sediments, *Geochim. Cosmochim. Acta*, 1996, vol. 60, no. 9, pp. 1479–1495.
4. Volkov, I.I. and Yagodinskaya, T.A., The Transitional Group Elements: Phosphorus, Rare Earth Elements, and Yttrium, *Litologiya i geokhimiya osadkov Tikhogo okeana (transtikhookeanskii profil')* (Lithology and Geochemistry of Pacific Ocean Sediments: The Transpacific Profile), Kholodov, V.N., Ed., Moscow: Nauka, 1979, pp. 203–224.
5. Koschinsky, A. and Halbach, P., Sequential Leaching of Marine Ferromanganese Precipitates: Genetic Implications, *Geochim. Cosmochim. Acta*, 1995, vol. 59, no. 24, pp. 5113–5132.
6. Dubinin, A.V., Ferromanganese Crust on Pelagic Sediments: Geochemistry and Formation Conditions, *Geokhimiya*, 1998, no. 11, pp. 1152–1163.
7. Dubinin, A.V. and Volkov, I.I., Mechanism of Rare Earth Element Accumulation on Oceanic Iron Hydroxides, *Geokhimiya*, 1989, no. 8, pp. 1089–1100.
8. Masuzawa, T. and Koyama, M., Settling Particles with Positive Ce Anomalies from the Japan Sea, *Geophys. Res. Lett.*, 1989, vol. 16, no. 6, pp. 503–506.
9. Sholkovitz, E.R., Landing, W.M., and Lewis, B.L., Ocean Particle Chemistry: The Fractionation of Rare Earth Elements between Suspended Particles and Seawater, *Geochim. Cosmochim. Acta*, 1994, vol. 58, no. 6, pp. 1567–1579.
10. Gromet, L.P., Dymek, R.F., Haskin, L.A., and Korotev, R.L., The "North American Shale Composite": Its Compilation, Major and Trace Element Characteristics, *Geochim. Cosmochim. Acta*, 1984, vol. 48, no. 12, pp. 2469–2482.
11. Dubinin, A.V. and Sval'nov, V.N., Differential Mobility of Iron Oxyhydroxides in the Micro- and Macronodule Formation Processes: Evidence from the Guatemala Basin, Pacific Ocean, *Dokl. Akad. Nauk*, 1996, vol. 348, no. 1, pp. 100–103.
12. Dubinin, A.V. and Sval'nov, V.N., Rare Earth Element Geochemistry of Micro- and Macronodules from the Bioproductive Zone of the Pacific Ocean, *Litol. Polezn. Iskop.*, 2000, no. 1, pp. 25–39.
13. Bogdanov, Yu.A., Gorshkov, A.I., Gurvich, E.G., *et al.*, Ferromanganese Crusts and Nodules from Guyots of the Northwestern Pacific, *Geokhimiya*, 1998, no. 5, pp. 518–531.
14. Elderfield, H., Hawkesworth, C.J., Greaves, M.J., and Calvert, S.E., Rare Earth Element Geochemistry of Oceanic Ferromanganese Nodules and Associated Sediments, *Geochim. Cosmochim. Acta*, 1981, vol. 45, pp. 513–542.
15. Elderfield, H. and Pagett, R., Rare Earth Elements in Ichthyoliths: Variations with Redox Conditions and Deposi-

tional Environment, in *The Science of the Total Environment*, 1986, vol. 49, pp. 175–197.

16. Dubinin, A.V., Skornyakova, N.S., Strekopytov, S.V., and Volkov, I.I., Rare Earth Element Geochemistry of Nodules and Sedimentary Host Rocks from the Northern Equatorial Pacific, *Litol. Polezn. Iskop.*, 1997, no. 2, pp. 199–211.
17. Dubinin, A.V. and Strekopytov, S.V., Rare Earth Element Geochemistry of the Formation of Ferromanganese Nodules in the Peru Basin, Pacific Ocean, *Litol. Polezn. Iskop.*, 1994, no. 4, pp. 17–32.
18. Fox, L.E., A Model for Inorganic Control of Phosphate Concentrations in River Waters, *Geochim. Cosmochim. Acta*, 1989, vol. 53, no. 2, pp. 417–428.
19. Buffle, J., de Vitre, R.R., Perret, D., and Leppard, G.G., Physicochemical Characteristics of a Colloidal Iron Phosphate Species Formed at the Oxic–Anoxic Interface of a Eutrophic Lake, *Geochim. Cosmochim. Acta*, 1989, vol. 53, no. 2, pp. 399–408.
20. Dubinin, A.V. and Volkov, I.I., Rare Earth Elements in the Metalliferous Sediments of the East Pacific Rise, *Geokhimiya*, 1986, no. 5, pp. 645–662.
21. Dubinin, A.V. and Volkov, I.I., Geochemistry of the Pelagic Sediments of the East Pacific Rise: Metalliferous Potential, *Litol. Polezn. Iskop.*, 1992, no. 6, pp. 3–24.
22. Dubinin, A.V. and Sval'nov, V.N., Evolution of Sedimentation: Evidence from Studies of Authigenic and Biogenous Phases in the Pelagic Sediments of the Pacific–Antarctic Depression, *Geokhimiya* (in press).
23. Dubinin, A.V. and Sval'nov, V.N., Rare Earth Element Geochemistry of Ferromanganese Micro- and Macronodules from the Nonproductive Zone of the Pacific Ocean, *Litol. Polezn. Iskop.*, 2000, no. 6, pp. 586–604.
24. Dubinin, A.V., Inductively Coupled Plasma Mass Spectrometry: Analysis of Rare Earth Elements in Reference Samples of Oceanic Sediments, *Geokhimiya*, 1993, no. 11, pp. 1605–1619.
25. Strekopytov, S.V. and Dubinin, A.V., Inductively Coupled Plasma Mass Spectrometry: Analysis of Zr, Hf, Mo, W, and Th in Reference Samples of Oceanic Sediments, *Zh. Anal. Khim.*, 1997, vol. 52, no. 12, pp. 1296–1298.
26. Sobolev, A.V., Melt Inclusions in Minerals as a Source of Principal Petrological Information, *Petrologiya*, 1996, vol. 4, no. 3, pp. 228–239.
27. Dubinin, A.V., Rare Earth Element Geochemistry of Oceanic Phillipsites, *Litol. Polezn. Iskop.*, 2000, no. 2, pp. 124–131.
28. Klinkhammer, G., Elderfield, H., and Hudson, A., Rare Earth Elements in Seawater near Hydrothermal Vents, *Nature* (London), 1983, vol. 305, no. 5931, pp. 185–188.
29. Boström, K., The Origin and Fate of Ferromanganoan Active Ridge Sediments, *Stockholm Contrib. Geol.*, 1973, vol. 27, no. 2, pp. 149–243.
30. Feely, R.A., Baker, E.T., Marumo, K., *et al.*, Hydrothermal Plume Particles and Dissolved Phosphate over the Superfast-Spreading Southern East Pacific Rise, *Geochim. Cosmochim. Acta*, 1996, vol. 60, no. 13, pp. 2297–2323.
31. Savenko, A.V., Phosphorous Coprecipitation with Iron Hydroxide Formed during Bottom Hydrothermal Solutions Interaction with Marine Water (Experimental Data), *Geokhimiya*, 1995, no. 9, pp. 1383–1389.
32. Staudigel, H. and Hart, S.R., Alteration of Basaltic Glass: Mechanisms and Significance for the Oceanic Crust–Sea-Water Budget, *Geochim. Cosmochim. Acta*, 1983, vol. 47, no. 2, pp. 337–350.
33. Lutts, B.G., *Geokhimiya okeanicheskogo i kontinental'nogo magmatizma* (Geochemistry of Oceanic and Continental Magmatism), Moscow: Nedra, 1980.